

Comparative Analysis of DMSP, MODIS, and GLOBSCAR

burn area estimation capabilities for Madagascar

by Nicholas J. Matzke

Graduate Student

U.C. Santa Barbara Geography Department

Research Completed Winter 2003

5722 Ellison Hall

U.C. Santa Barbara

Santa Barbara, CA, 93106

Phone: (805) 961-9947

Fax: (805) 893-3146

Email: matzke@geog.ucsb.edu

January 2003

ABSTRACT

Comparative Analysis of DMSP, MODIS, and GLOBSCAR burn area estimation capabilities for Madagascar

Madagascar is a biodiversity hotspot and anthropogenic fire is an important factor in land cover change that needs to be better understood. Several coarse resolution fire products, including those derived from GLOBSCAR, MODIS and DMSP-OLS, have recently become available for Madagascar. However, the relative strengths and weaknesses of these products have not been rigorously assessed. This study compares GLOBSCAR-, DMSP- and MODIS-derived fire products with each other and with burn area maps derived from Landsat ETM. An assessment of the usage of geostatistical vs. more classical statistical methods of raster comparison is then presented, and an assessment of the utility of coarse-resolution fire products is made.

INTRODUCTION

In recent years, several coarse-resolution active fire products have been developed for the purposes of global fire mapping. The various products are reviewed by Fuller (2000), however extant work comparing multiple fire products has been published. A preliminary comparison of three coarse-resolution fire products is presented here.

Madagascar is the world's fourth largest island, with an area of 587,000 ha. Anthropogenic biomass burning in Madagascar has been continual source of contention between rural resources and government authorities since pre-colonial times due to concerns about forest loss and other environmental damage. The historical, political, and social dynamics of the topic have been reviewed in considerable detail by Kull (2000; 2002). However, in his review of annual governmental burn area statistics Kull concluded that available numbers were no reliable estimates of burn area were available. Some authorities (Jolly 1990) and many secondary sources (e.g., Tyson 2000) put the annual area burned in Madagascar at the astounding figure of *one-third*. However, these figures appear to be wild guesses at best and never cite any hard data.

The fire season in Madagascar is bimodal, reflecting the physical geography. The modes of burning vary between the western grassland and savanna, and the eastern slope (Randriambelo *et al.* 1998). The dominant topographic feature in Madagascar is the eastern mountain chain, which runs 1600 km from the northeast to southeast. West of the mountains lies a high (over 1000 m) central plateau, primarily now secondary grassland, with occasional fire-resistant tree species. Along the west coast remain significant patches of dry deciduous forest, and in the south lies the famous xerophyllous spiny forest. While the spiny forest is considered too dry (Jolly *et al.* 1984) for wildfires (although not collection for fuelwood or charcoal production), the grasslands and savannas experience the vast majority of the annual area burned. The peak of the fire season is September, as fires are lit primarily to bring up a "green bite" for cattle (although fires have a large number of uses in Madagascar, reviewed by Kull 2000). Most of the rest of the fires occur in August and October, however burning will begin at low levels beginning with the end of the rainy season, approximately in June. The end of the dry season, approximately in November, marks the end of burning in the grasslands.

Essentially the entire eastern slope was once covered with rainforest, but most of this has been lost due to logging and slash-and-burn cultivation, known locally as *tavy* (Green and Sussman 1990; Sussman *et al.* 1994, 1996). The prevailing easterly tradewinds bring moisture from the Indian Ocean, which interact with mountains to produce regular orographic precipitation along the eastern slope for almost the entire year. The tradewinds slacken in October, and the reversal in air flow brings descending, drying winds from the west (Battistini 1972, Donque 1972, Randriambelo *et al.*, 1998). October and early November are thus the primary months for *tavy* burning.

Randriambelo *et al.* (1998) published monthly active fire counts detected with 1995 AVHRR data for Madagascar. They give some sense of the temporal distribution of fires on a national scale (see Figure 1).

METHODS

Landsat ETM+

Landsat Enhanced Thematic Mapper is a well known high-resolution sensor that does not need to be reviewed here. For purposes of DMSP assessment, the USGS purchased a pair of images from path 158, row 73, a region of central eastern Madagascar covering the coast, the port city of Toamasina, a portion of the mountain rainforest including the national park Andasibe, and a region east of the mountains containing grassland and plantations (location shown in Figure 7). The image dates (the only relatively cloud-free images available for that year) were April 19, 2000 (well before the fire season) and October 28, 2000 (just following the peak of the fire season).

Spectral Mixture Analysis (Adams *et al.* 1995) was applied using endmembers derived from the reference image (Path 158, row 73, 10/28/00). The images were unmixed into endmember fractions of shade, green vegetation, non-photosynthetic vegetation, and soil. Potential image endmember spectra were identified through examination of 2-D plots of DN values (e.g., band 3 vs. band 4, 5 vs. 4, 5 vs. 3, etc.) and several combinations were rejected after trial-and-error unmixing runs. Spectral mixture analysis is not a required step for producing a remotely-sensed map, as an automated classifier can easily be applied to raw Landsat imagery. However, conducting spectral mixture analysis prior to classification serves several purposes, as in one step it provides a method to reduce dimensionality of the dataset, intercalibrate images from multiple dates and locations, and improve image interpretability (Adams *et al.* 1995).

The images were classified using a binary decision tree (a supervised classifier) into ten classes, followed by a 3x3 majority filter. The tree used is shown in . There were essentially no burns on the April 19, 2000 image (in other cases where the image dates were closer together, on 1999 imagery used for another study, the burn scars from the first image were subtracted. Clouds were flagged as nodata pixels. Due to space limitations a full accuracy assessment is not presented here, however the overall accuracy statistics were reasonable (overall accuracy = 80.46%, kappa statistic = 0.773), even if similar classes were not combined. When similar classes were combined, resulting in six classes, overall statistics improved (overall accuracy = 86.00%, kappa statistic = 0.811). The classification and accuracy assessment are described in more detail in Matzke (2003).

Following classification, the ETM-mapped burnscars were extracted to a separate layer. The burnscar map was then resampled from 30 m to 1 km (resulting in a fraction area burned for each 1 km pixel). Fine-resolution nodata pixels were excluded from the calculation (the 1 km pixel fraction being calculated from the remaining 30 m pixels), and 1 km pixels that were majority-nodata were themselves flagged as nodata. The same procedure was followed in averaging the 1 km map to 3 km to match with the other data.

MODIS

MODIS, the MODerate-Resolution Imaging Spectrometer, is onboard the Terra (morning equator overpass) and

Aqua (afternoon equator overpass) platforms as part of NASA's Earth Observing System. Data is acquired in 36 bands appropriate for a wide range of purposes (see <http://modis-land.gsfc.nasa.gov/> for a listing of the land products). The MODIS Thermal Anomalies products (Owens 2001) detect active fires using the bands at 4 and 11 micrometers via a thresholding algorithm, reviewed by Kaufman and Justice (1998); the basic theory is given by Dozier (1981), see also Chuvieco (Chuvieco 1999).

The only MODIS-derived Thermal Anomalies product available for the Madagascar fire season in 2000 is MOD14A2 (<http://edcdaac.usgs.gov/modis/mod14a2.html>). This product is the composite 8-day fire product (current MODIS fire product availability can be checked at http://modis.gsfc.nasa.gov/data/dataproducts.php?MOD_NUMBER=14). This product has "minimally validated" beta status beginning on August 20, 2000, and validated status beginning November 1, 2000. Product resolution is 1 km. For each pixel, the 8-day composite product contains a record of the "most confident detected fire" detected over the 8-day period, or if no fire is detected, an "unknown" or landcover classification is given. The pixel assignments are shown in Table 1. Some preliminary literature on evaluation and use of the MODIS fire product is available (Justice *et al.* 2002; Kaufman and Justice 1998; Roy *et al.* 2002).

The MODIS MOD14A2 product was downloaded from the USGS Eros Data Center, the data was extracted from the HDF file format and reprojected into the standard projection for all Madagascar datasets (Hotine Oblique Mercator, or HOM). Seventeen 8-day composite images were available for the period of August 20, 2000 to December 31, 2000. Interestingly, in the fire product the only pixels flagged as fire were all given classification 8, "nominal confidence fire", perhaps an indication of the in-progress status of the MODIS Thermal Anomalies product validation.

The pixels tagged as fires across the seventeen dates were summed to give a "total recorded fires per pixel" map for the 2000 fire season. This 1 km map was then resampled to a range of coarser resolutions via averaging to match the other datasets.

ATSR-2 GLOBSCAR

ATSR-2, the second Advanced Along-Track Scanning Radiometer, is onboard ERS-2. It has seven channels (2 visible, 2 NIR, and 3 TIR) and produces a 1-km resolution image of a region every 3 days (for more details see Arino *et al.* 2001). ATSR-2 can be used for both active fire detection and burn scar mapping (GLOBSCAR). The current assessment examines only the GLOBSCAR product. The monthly GLOBSCAR product for 2000, for all of Africa including Madagascar, can be seen online at: <http://dup.esrin.esa.it/projects/isummaryp24.asp>.

The preliminary algorithm for flagging burnt pixels is described by Arino *et al.* (2001). Two algorithms are employed, K1 and E1. K1 identifies burnt pixels as those that deviate from cluster of the rest of the image via low NIR reflectance (burned vegetation has decreased reflectance in these wavelengths due to the presence of char and

ash) and high TIR signal (high brightness temperature due to the lower albedo burned surfaces, which results in a higher absorption of solar radiation and therefore higher brightness temperature). The second algorithm, E1, is used in equatorial zones with high fire activity. The tests applied are given in Figure 6.

The preliminary fire scar product for Madagascar (Jan. - Dec. 2000) was provided by Muriel Simon of the ESA. It should be emphasized (Simon, personal communication) that the product is preliminary and the algorithm was designed to minimize commission errors (minimize false fires) at the expense of omission errors (increasing missed fires). The file was in ASCII text format, with one line per pixel. 8972 pixels were identified as burned over the course of the year. The only information given in this file was the detection date, and latitude and longitude. Thus this particular product did not contain information as to which algorithm was used in particular places. A product with more details is available (Simon, personal communication) but for the purposes of a preliminary evaluation this was deemed sufficient.

The ASCII burn scar pixel coordinates were imported into ArcView shapefile format. As a few pixels were flagged as burned in repeated months, the shapefile was split into months. As DMSP-OLS and MODIS data was only available for August-December 2000, only the last five months of GLOBSCAR data were selected for further analysis. Each month's data was converted to 1 km grids with individual pixels flagged as burned (1) or not burned (0). The five-month dataset was then summed in to produce two cumulative data products: a three-month "total pixels with detected burn scar" map for August-October (to match the Landsat ETM-derived burn area map), and a five-month version of the product to match with DMSP-OLS and MODIS.

In order to match the other datasets, the 1 km grids were resampled (via averaging) to a range of coarser resolutions. As the georectification accuracy of the preliminary product was approximately 2-3 km (Simon, personal communication), plus whatever additional uncertainties resulted from converting the lat-long coordinates to a projected grid, this was deemed a minimal sacrifice. Coarsening the 1 km product also had the advantage of changing the binary (0 vs. 1) dataset into a slightly more continuous dataset (decimals ranging from 0 to 1).

DMSP-OLS

The Operational Linescan System, or OLS, is a VNIR sensor aboard the Defense Meteorological Satellite Program (DMSP) satellites (currently functioning in orbit are F-12, F-13, and F-15, according to <http://www.isciences.com/NewSite/sensors/current.html>). These satellites are essentially U.S. Defense Department weather satellites and have been operational since the early 1970's (Croft 1973). The primary purpose of the OLS VNIR channel is to detect clouds by moonlight, so the sensitivity is very high. In addition to clouds, gas flares, lightning, city lights, and fires can be detected with DMSP-OLS. However, the channel has a radiometric resolution of only 64 DN values and is easily saturated by bright emissions sources. Additional issues such as a fire "blowing up" into several pixels (Kihn 1996), cloud cover, variable gain and variable threshold above background brightness for flagging fire pixels, make *a priori* interpretation of DMSP-OLS data difficult. However, a significant literature

exploring the usage of DMSP-OLS has been developed by Elvidge and colleagues (Elvidge and Baugh 1996; Elvidge *et al.* 2001; Elvidge *et al.* 1996) and with some success in estimating burn area from DMSP-OLS (Elvidge, 2001). A TIR channel also exists but it is not usually used due to saturation issues.

The product used in this study was a set of 169 images (0-2 per night) covering the time period for which the USGS had purchased the DMSP-OLS fire product (developed by Chris Elvidge of NOAA, see <http://www.ngdc.noaa.gov/dmsp/fires/globalfires.html>) for Madagascar in 2000 (August 1-December 31). Given the difficulties in interpreting DN values, any pixel with a DN of 5 or higher was counted as a fire detection (apart from 0, the minimum DN value in the product was 5). This fire count product was combined with a cloud-count product to produce a fire activity index map for any given period within the available data, using the following formula:

$$x_{cu}(\mathbf{u}) = a(\mathbf{u}) / [T - c(\mathbf{u})] \quad (1)$$

where:

$x_{cu}(\mathbf{u})$ = cumulative fire index at grid location \mathbf{u} .

$a(\mathbf{u})$ = number of detected fires over the time period of interest

$c(\mathbf{u})$ = number of detected clouds for the entire fire season

T = total number of observations for the entire fire season

The resolution of the NOAA DMSP-OLS fire product is approximately 1 km, however the resolution of the raw DMSP-OLS data is actually 2.7 km. Additionally the "blowing up" discussed by Kihn (1996) and any additional scattering due to smoke or haze produce a product smoother than reality. Therefore before comparison was performed, the 1 km fire index was coarsened to various resolutions via averaging. The MODIS, GLOBSCAR, and ETM-derived products were similarly coarsened via averaging (for MODIS and GLOBSCAR, this resulted in coarse pixels with values representing the number of 1 km pixels scored as burned, divided by the total number of pixels).

The burn products for the entirety of Madagascar for August-October 2000 are displayed in Figure 7. The burn products for the area covered by the Landsat reference image are displayed in Figure 8. As the histogram stretch strongly influences the display of the ETM-derived percent burn area image, several displays of this image are shown in Figure 9.

Analysis

The three coarse-resolution fire products were compared to the Landsat ETM-derived burn area map. In order to match the approximate timespan of the ETM-derived image, the summary products as shown above were calculated for the approximate period August 1 -- October 28, or as close to this as the various products would allow.

Although the first image of the Landsat image was dated in April, as this path-row is located in eastern Madagascar it can be fairly safely assumed that few to no fires occurred before August in this scene (Randriambelo *et al.* 1998).

To test the key effect of comparison at varying resolution, a series of MATLAB scripts were written that took the 1 km raster maps derived from ETM, DMSP, MODIS, and GLOBSCAR, and resampled them (via averaging) at 1 km increments from 1 km resolution (190 x 201 pixels) to 90 km resolution (a 2 x 2 raster). Each of the three secondary datasets was then used to predict ETM burn area on a per-pixel basis, and the regression parameters and significance measures for all 180 regressions (90 x 3) were recorded and plotted.

In order to summarize the large number of analyses performed, r^2 , slope, and p-value of the regression slope were plotted as a function of pixel resolution. The results were compared to previous work using geostatistics and Sequential Gaussian Simulation with the DMSP product as a secondary dataset (Matzke 2003).

RESULTS

Figure 10 shows the results of regression of each of the three coarse-resolution fire products against ETM-derived burn area at various scales. Using DMSP as a predictor, correlation appears to improve from resolutions of 1-5 km, then levels off or drops for much coarser resolutions, but spikes at 60 km resolution. A similar pattern is seen for the MODIS and GLOBSCAR fire product predictors, although the DMSP almost universally shows a better correlation than MODIS, and both consistently outperform GLOBSCAR.

A better survey of the analysis is shown in Figure 11. Although for all predictors there appears to be an improvement in correlation as resolution coarsens, the trend is severely interrupted by sudden drops that persist for substantial resolution intervals. However, the same order of predictor usefulness (DMSP > MODIS > GLOBSCAR) is followed throughout.

A similar plot of slope vs. resolution shows that, while slope shows more stability than r^2 , it is still significantly influenced by resolution. For the DMSP case, the slope of the regression line begins at ~2, but increases, with much variation, to ~4 with 25 km resolution and to ~6 at 35 and 60 km resolution. Above 80 km, the slope of the regression actually becomes negative.

The plot of p-value vs. slope (Figure 11) reveals that most of the slopes are significantly different from zero at the 0.05 significance level except for the resolution ranges 40-50 km and resolution greater than 65 km.

The MODIS and GLOBSCAR plots are somewhat similar to the DMSP plot in their pattern of p-value vs. resolution, however in general the p-values are higher and exceed the 0.05 threshold more frequently.

A plot of y-intercept vs. resolution (not shown) places the y-intercept very near zero for those regressions with low p-values.

CONCLUSION

This study emphasizes the importance of the Modifiable Unit Area Problem (MAUP) and aggregation effect (O'Sullivan and Unwin 2003; Quattrochi and Goodchild 1997). The parameters of linear models fit to spatial datasets vary widely, often changing drastically with “small” changes in pixel block size due to reconfiguration of the coarse pixels (e.g., moving from a 4x4 to a 3x3 coarse grid). This can be seen in Figure 11, where n is plotted on a log scale, and drastic oscillations in parameters co-occur with shifts in n .

This study also gives some indication of the difficulties of using traditional statistics for comparing spatial datasets. At high resolutions, n is so large that even a regression that explains only 10% of the variance (e.g., for DMSP predicting burn area at 1 km resolution) will have a high statistical significance as measured by p . Low resolutions produce a reasonable number of data points to regress but sensitivity to slightly different configurations of the coarse pixels can result in erratic results.

In this context, geostatistical techniques are an oft-recommended solution to the problem (O'Sullivan and Unwin 2003). However, the most common standard technique for assessing spatial cross-correlation between datasets, the Linear Model of Coregionalization, or LMC (Deutsch and Journel 1998; Goovaerts 1997) only results in structural correlation coefficients for each of the variogram structures used to model the empirical variograms and cross-variograms. While the author has employed this technique for the comparison of two datasets, ETM-mapped burn area and the DMSP fire product (Matzke 2003), the LMC process is somewhat subjective and unless the structures can be directly tied to physical processes producing structure at specific scales (e.g., Dobermann *et al.* 1995), the results are ambiguous. In addition, the process becomes onerous when dealing with more than two datasets which are a mixture of discrete and continuous data (as is the situation with many fire products). A major advantage of LMC is that the resultant variograms can be used in geostatistical simulation models, permitting a robust assessment of uncertainty; the author has used this technique to estimate an annual burn area for Madagascar of 6-7% (Matzke 2003) using the DMSP fire product as conditioning secondary data. One result that is clear thus far from the studies of coarse resolution burn products is that predicting burn area on fine scales, e.g. preserves in Madagascar, is a dubious exercise. Province- or national- scale burn area estimates are a reasonable goal.

However, despite the somewhat erratic results retrieved by classical techniques, this paper clearly shows that the DMSP fire product is significantly superior to the other coarse resolution fire products available for 2000. It should be stressed that both the 2000 MODIS and GLOBSCAR products were the first fire products available from their respective sensors; starting in 2001 numerous additional products have become available. The methods and programs developed in this study contribute to the toolkit of geographers attempting to evaluate the value of various coarse-resolution fire products for predicting burn area.

REFERENCES

- Adams, J. B., Sabol, D. E., Kapos, V., Almeida, R., Roberts, D. A., Smith, M. O. and Gillespie, A. R. (1995). "Classification of Multispectral Images Based on Fractions of Endmembers - Application to Land-Cover Change in the Brazilian Amazon." *Remote Sensing of Environment* **52**(2): 137-154.
- Arino, O., Simon, M., Piccolini, I. and Rosaz, J.-M. (2001). "The ERS-2 ATSR-2 World Fire Atlas and the ERS-2 ATSR-2 World Burnt Surface Atlas Projects." Accessed online: Oct. 15, 2002. URL: http://shark1.esrin.esa.it/ionia/FIRE/DOCS/Arino_Aussois2001.doc.
- Chuvieco, E., Ed. (1999). *Remote Sensing of Large Wildfires in the European Mediterranean Basin*. Berlin, Springer.
- Deutsch, C. V. and Journel, A. G. (1998). *GSLIB geostatistical software library and user's guide*. New York, Oxford University Press.
- Dobermann, A., Goovaerts, P. and George, T. (1995). "Sources of soil variation in an acid Ultisol of the Philippines." *Geoderma* **68**: 173-191.
- Dozier, J. (1981). "A method for satellite identification of surface temperature fields of subpixel resolution." *Remote Sensing of Environment* **11**: 221-229.
- Elvidge, C. D. and Baugh, K. E. (1996). Survey of fires in Southeast Asia and India during 1987. *Biomass Burning and Global Change*. J. S. Levine. Cambridge, MIT Press. **1**: 73-85.
- Elvidge, C. D., Hobson, V. R., Baugh, K. E., Dietz, J. B., Shimabukuro, Y. E., Krug, T., Novo, E. M. L. M. and Echavarría, F. R. (2001). "DMSP-OLS estimation of tropical forest area impacted by surface fires in Roraima, Brazil: 1995 Versus 1998." *International Journal of Remote Sensing* **22**(14): 2661-2673.
- Elvidge, C. D., Kroehl, H. W., Kihn, E. A., Baugh, K. E., Davis, E. R. and Hao, W. M. (1996). Algorithm for the Retrieval of Fire Pixels from DMSP Operational Linescan System Data: Remote Sensing, Modeling and Inventory Development, and Biomass Burning in Africa. *Biomass Burning and Global Change*. J. S. Levine. Cambridge, MIT Press. **2**: 73-84.
- Fuller, D. O. (2000). "Satellite remote sensing of biomass burning with optical and thermal sensors." *Progress in Physical Geography* **24**(4): 543-561.
- Goovaerts, P. (1997). *Geostatistics for natural resources evaluation*. New York, Oxford University Press.
- Green, G. M. and Sussman, R. W. (1990). "Deforestation History of the Eastern Rain Forests of Madagascar from Satellite Images." *Science* **248**(4952): 212-215. URL: <http://www.jstor.org/journals/00368075.html>.
- Jolly, A. (1990). On the edge of survival. *Madagascar: A World Out of Time*. F. Lanting. New York, Aperture: 110-121.
- Jolly, A., Oberle, P. and Albignac, R., Eds. (1984). *Madagascar*. Key Environments. Oxford, Pergamon Press.
- Justice, C. O., Giglio, L., Korontzi, S., Owens, J., Morisette, J. T., Roy, D., Descloitres, J., Alleaume, S., Petitcolin, F. and Kaufman, Y. (2002). "The MODIS fire products." *Remote Sensing of Environment* **83**(1-2): 244-262.
- Kaufman, Y. J. and Justice, C. O. (1998). "Algorithm Technical Background Document: MODIS FIRE PRODUCTS (Version 2.2)." Accessed online: Oct 15. URL: http://modis.gsfc.nasa.gov/data/atbd/atbd_mod14.pdf.

- Kihn, E. A. (1996). Forest Fire Detection from DMSP Operational Linescan System (OLS) Imagery. *Biomass Burning and Global Change: Remote Sensing, Modeling and Inventory Development, and Biomass Burning in Africa*. E. Levine. Cambridge, MIT Press. **1**: 86-91.
- Kull, C. A. (2000). Isle of Fire: The Political Ecology of Grassland and Woodland Burning in Highland Madagascar. *Department of Environmental Science, Policy, and Management*. Berkeley, CA, University of California at Berkeley.
- Kull, C. A. (2002). "Madagascar's burning issue: the persistent conflict over fire." *Environment* **44**(3): 8-19.
- Matzke, N. (2003). Remote Sensing and Geostatistical Analysis of Anthropogenic Biomass Burning and Forest Degradation in Madagascar. Geography Department. Santa Barbara, California, University of California, Santa Barbara.
- O'Sullivan, D. and Unwin, D. J. (2003). *Geographic Information Analysis*. Hoboken, New Jersey, John Wiley & Sons.
- Owens, J. (2001). "MODIS Fire and Thermal Anomalies Products." Accessed online: 5/28/2001. URL: <http://modis-fire.gsfc.nasa.gov/>.
- Quattrochi, D. A. and Goodchild, M. F. (1997). *Scale in Remote Sensing and GIS*. New York, CRC Press.
- Randriambelo, T., Baldy, S. and Bessafi, M. (1998). "An improved detection and characterization of active fires and smoke plumes in south-eastern Africa and Madagascar." *International Journal of Remote Sensing* **19**(14): 2623-2638.
- Roy, D., Lewis, P. E. and Justice, C. O. (2002). "Burned area mapping using multi-temporal moderate spatial resolution data—a bi-directional reflectance model-based expectation approach." *Remote Sensing of Environment* **83**(1-2): 263-286.
- Sussman, R. W., Green, G. M. and Sussman, L. K. (1994). "Satellite Imagery, Human Ecology, Anthropology, and Deforestation in Madagascar." *Human Ecology* **22**(3): 333-354.
- Sussman, R. W., Green, G. M. and Sussman, L. K. (1996). The Use of Satellite Imagery and Anthropology to Assess the Causes of Deforestation in Madagascar. *Tropical Deforestation: The Human Dimension*. L. E. Sponsel, T. N. Headland and R. E. Bailey. New York, Columbia University Press: 296-315.
- Tyson, P. (2000). *The Eighth Continent : Life, Death, and Discovery in the Lost World of Madagascar*. New York, Avon Books.

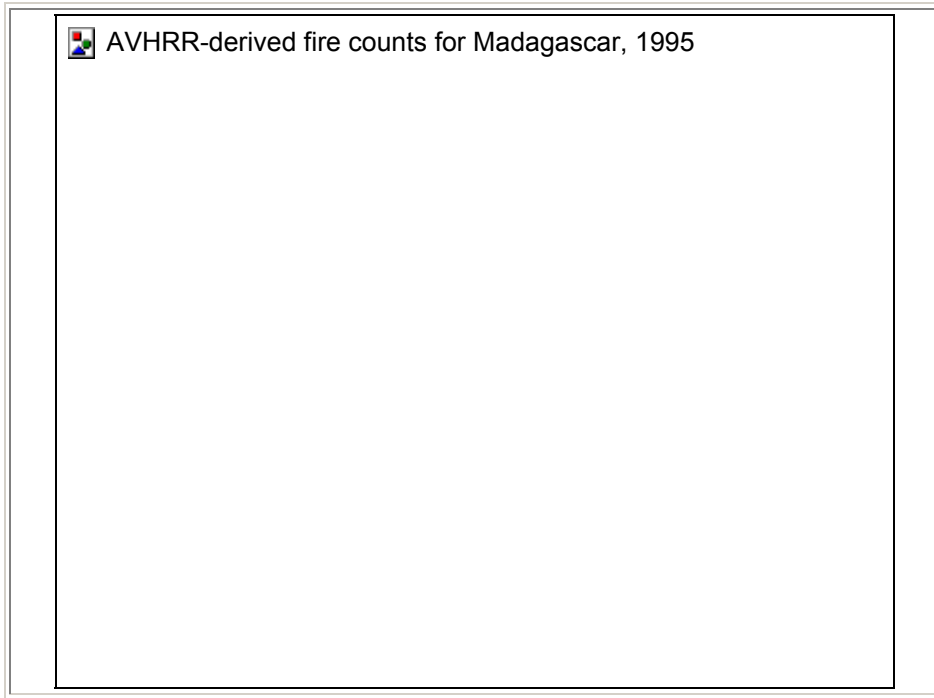


Figure 1: AVHRR-derived fire counts for Madagascar, 1995

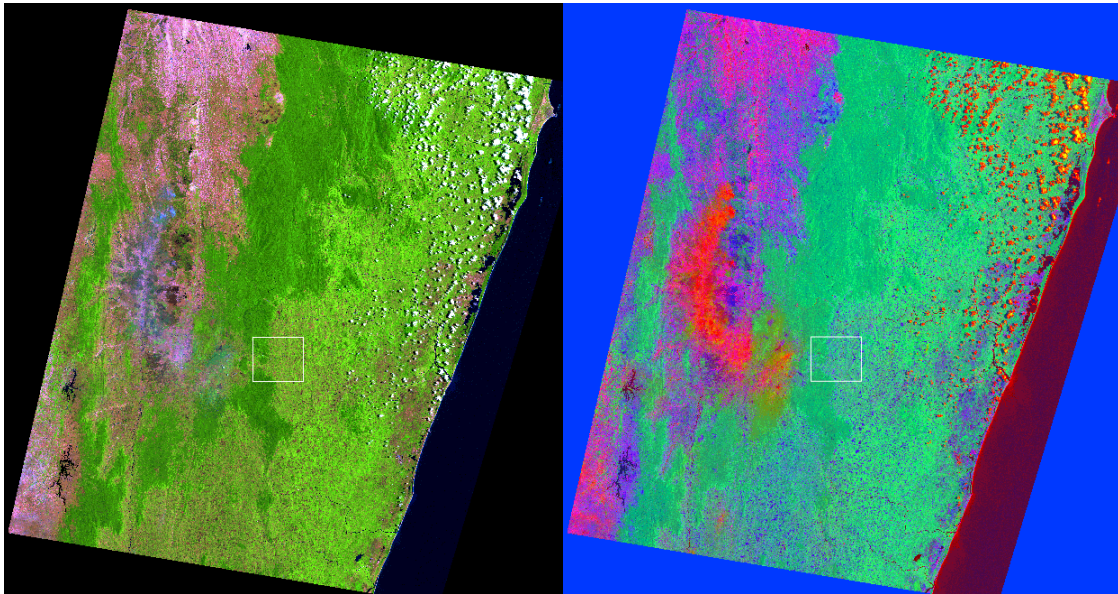


Figure 2: Path 158, row 73, October 28, 2000. *Left:* Landsat ETM false-color composite, RGB: 543. The dark areas in the center-left portion of the image are large burnscars. *Right:* Endmember fractions image: RGB: Soil, green vegetation, non-photosynthetic vegetation. White box is shown enlarged in Figure 3. The presence of haze/smoke is revealed in the fractions images, represented by the red (high soil fraction) smudge just to the west of the location of the large burnscars.

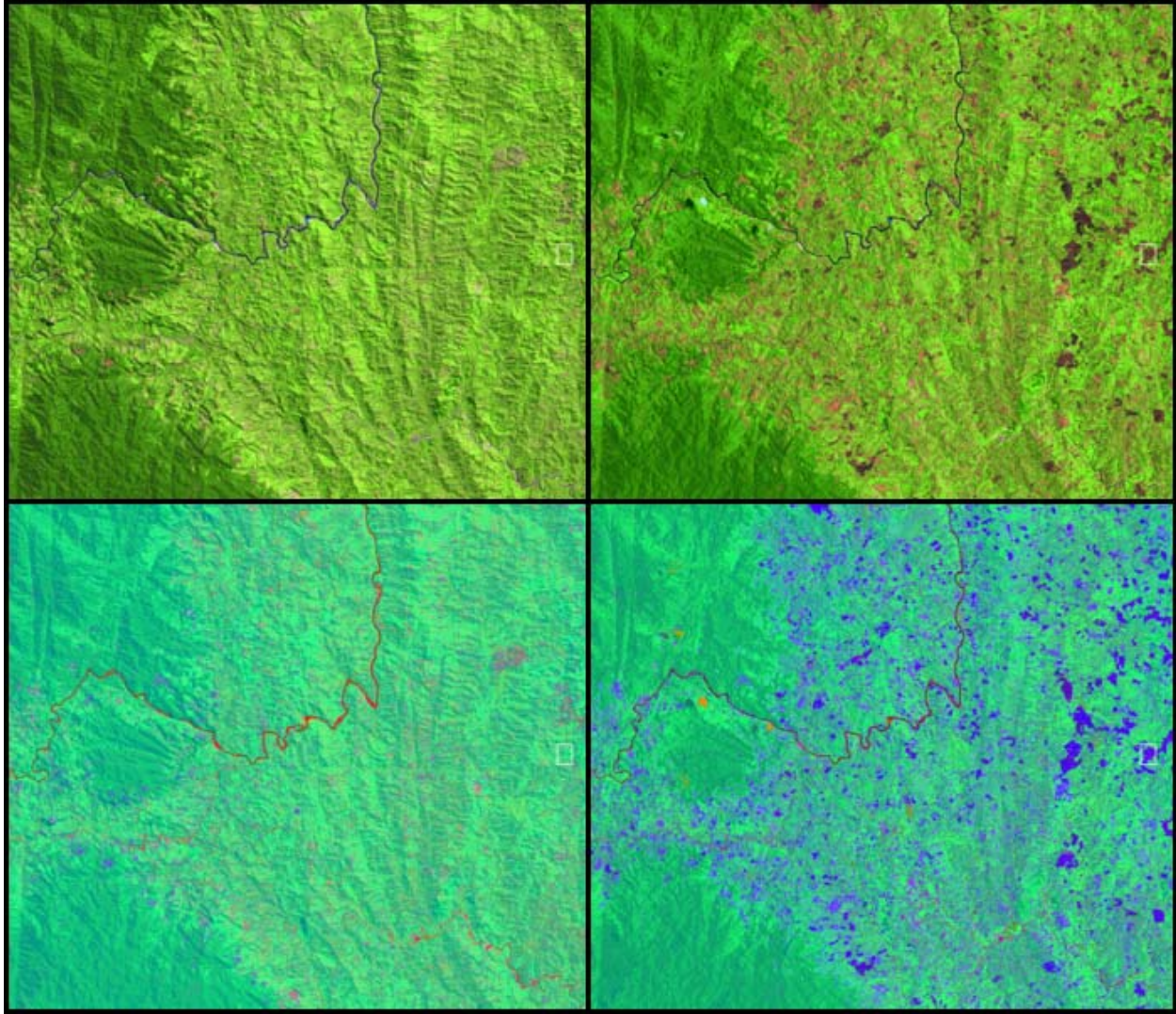


Figure 3: Enlargement of region delineated in **Figure 2**. Top row: Landsat images. Bottom row: Endmember fractions. Left column: Pre-fire season, April 19, 2000. Right column: End fire season, October 28, 2000.

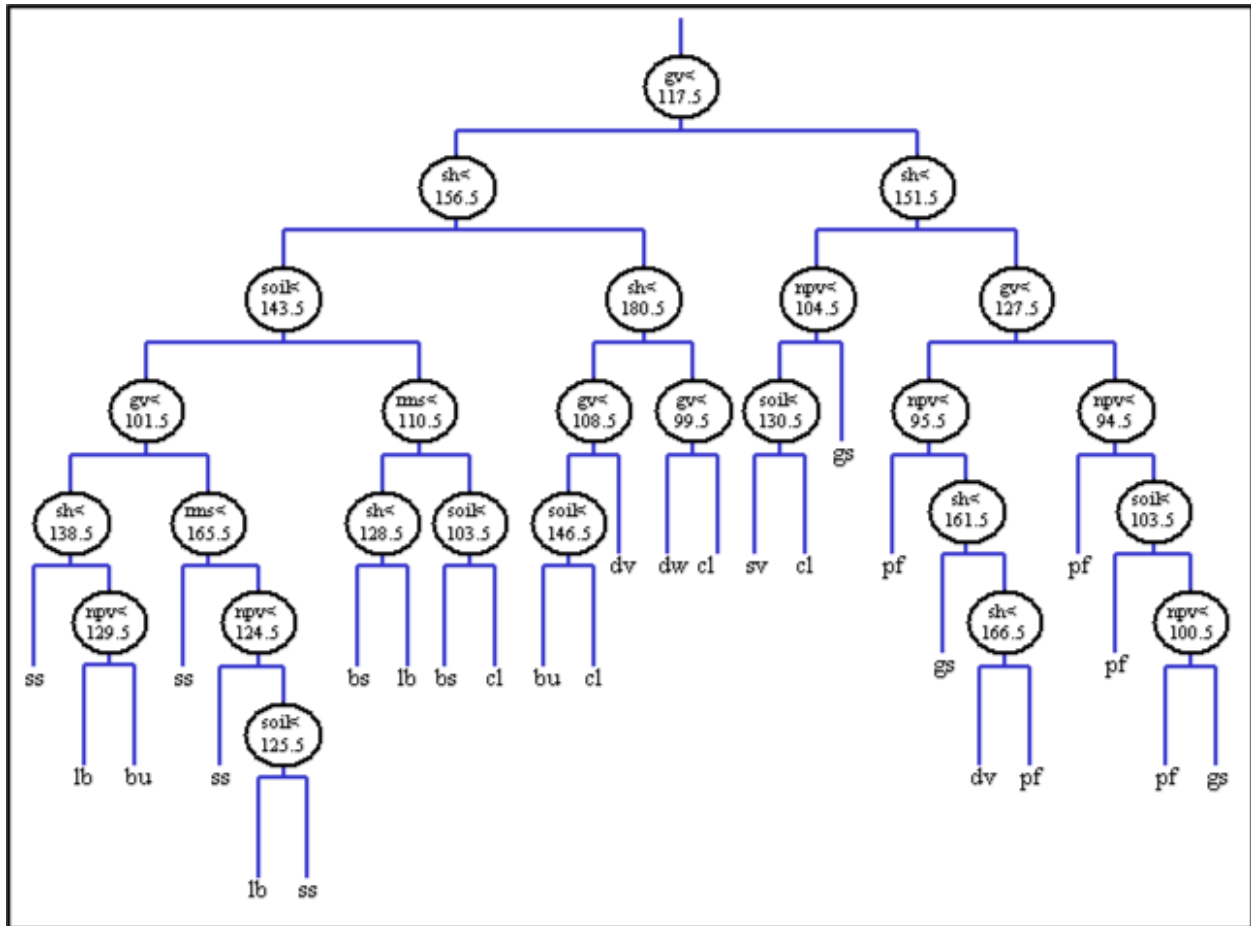


Figure 4: Final binary decision tree. The decision rules are shown in ovals, the output class abbreviations (described in text) are the "leaves" of the tree. For every decision, the left branch is followed if the pixel is less than the specified value, and the right branch is followed if the pixel value is higher. Class abbreviations on the leaves of the tree are defined in **Figure 5**.

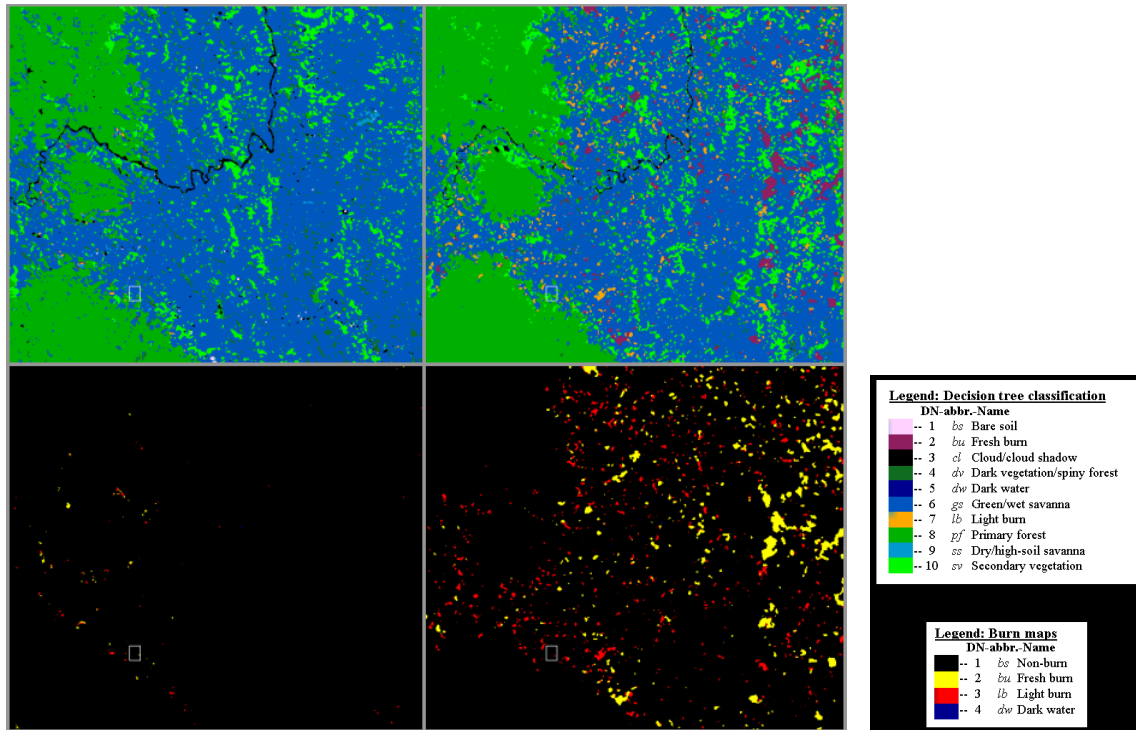


Figure 5: Same region as **Figure 3**. Top row: landcover map resulting from final decision tree classification. Bottom row: Extracted burn scars (yellow = fresh burn, red = light burn, black = unburned). Left column: April 19, 2000. Right column: October 28, 2000.

Table 1: Pixel assignments in the MOD14A2 fire product (source: Owens 2001)

Pixel Value	Meaning
0	not processed (missing input data)
2	not processed (other reason)
3	water
4	cloud
5	no fire
6	unknown
7	low-confidence fire
8	nominal-confidence fire
9	high-confidence fire

1. BT 11 micron > 300K
2. NDVI < 1400
3. MVI > 1000
4. Reflectance SWIR 1.6 micron < 20 %
5. Reflectance NIR 0.87 micron < 25 %
6. Reflectance RED < 10 %

Where:

$$\text{NDVI} = 1000 * \left\{ \left[\frac{\text{NIR} - \text{RED}}{\text{NIR} + \text{RED}} \right] + 1 \right\}$$

$$\text{MVI} = 1000 * \left\{ \left[\frac{\text{SWIR} - \text{NIR}}{\text{SWIR} + \text{NIR}} \right] + 1 \right\}$$

Figure 6: E1 algorithm parameters as given in Arino *et al.* (2001).


 Animation of DMSP, MODIS, and GLOBSCAR-derived fire maps, Aug-Dec 2000, 3km resolution

Figure 7: Side-by-side comparison of DMSP, MODIS, and GLOBSCAR-derived fire maps, Aug-Dec 2000, 3km resolution. Box outline represents approximate position of Landsat 7 WRS path 158, row 73.

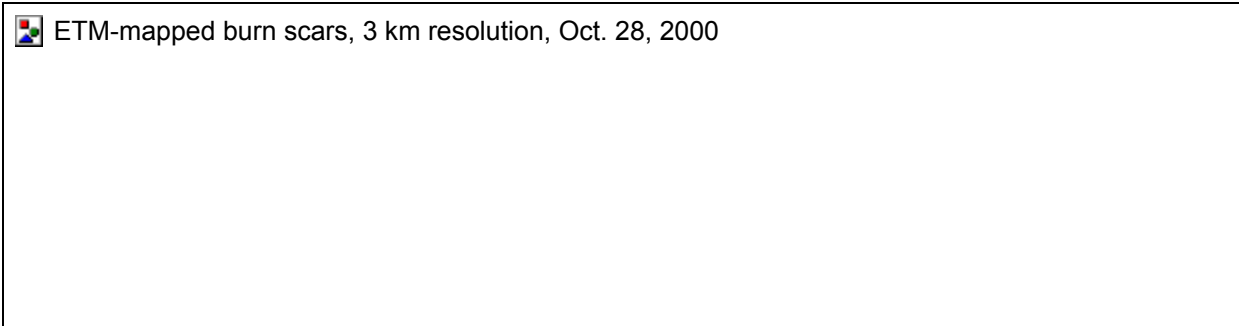


Figure 8: In order: ETM fraction burn area, DMSP-OLS fire index, MODIS fire detection count, and GLOBSCAR-derived firescar detection count, Aug-Oct 2000, 3km resolution. Landsat 7 WRS path 158, row 73. Red represents nodata on Landsat scene.

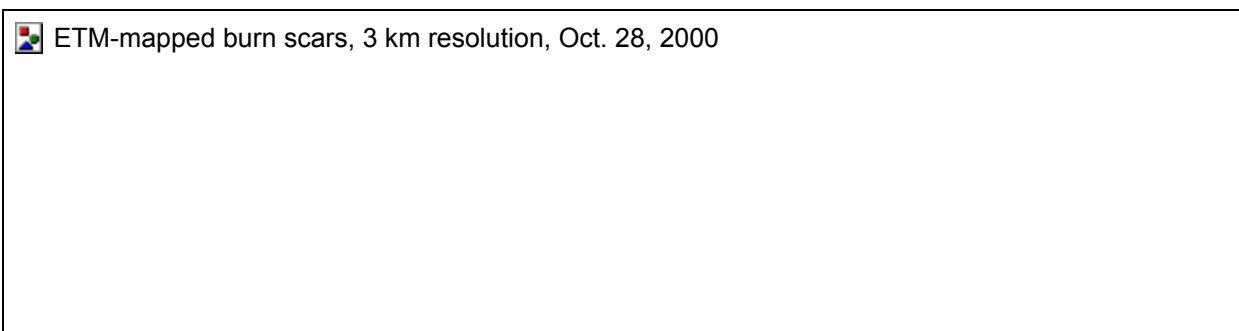


Figure 9: ETM fire maps, with different stretches, Aug-Oct 2000, 3km resolution. Landsat 7 WRS path 158, row 73. Red represents nodata on Landsat scene.

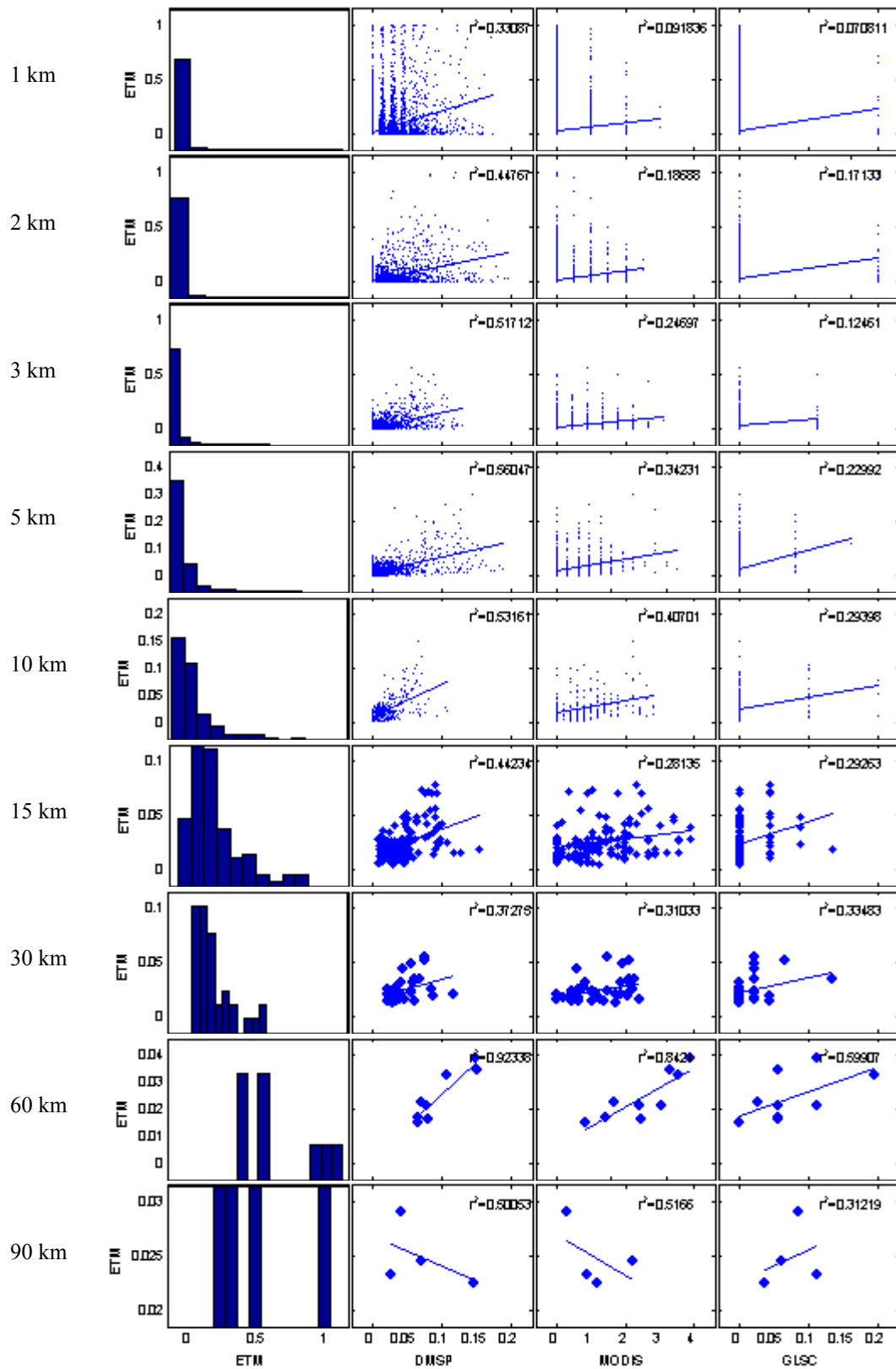


Figure 10: Selected regressions as resolution coarsens. In some cases correlation improves with larger pixels, but the trend is not constant. First column contains the histograms of ETM-derived burn area.

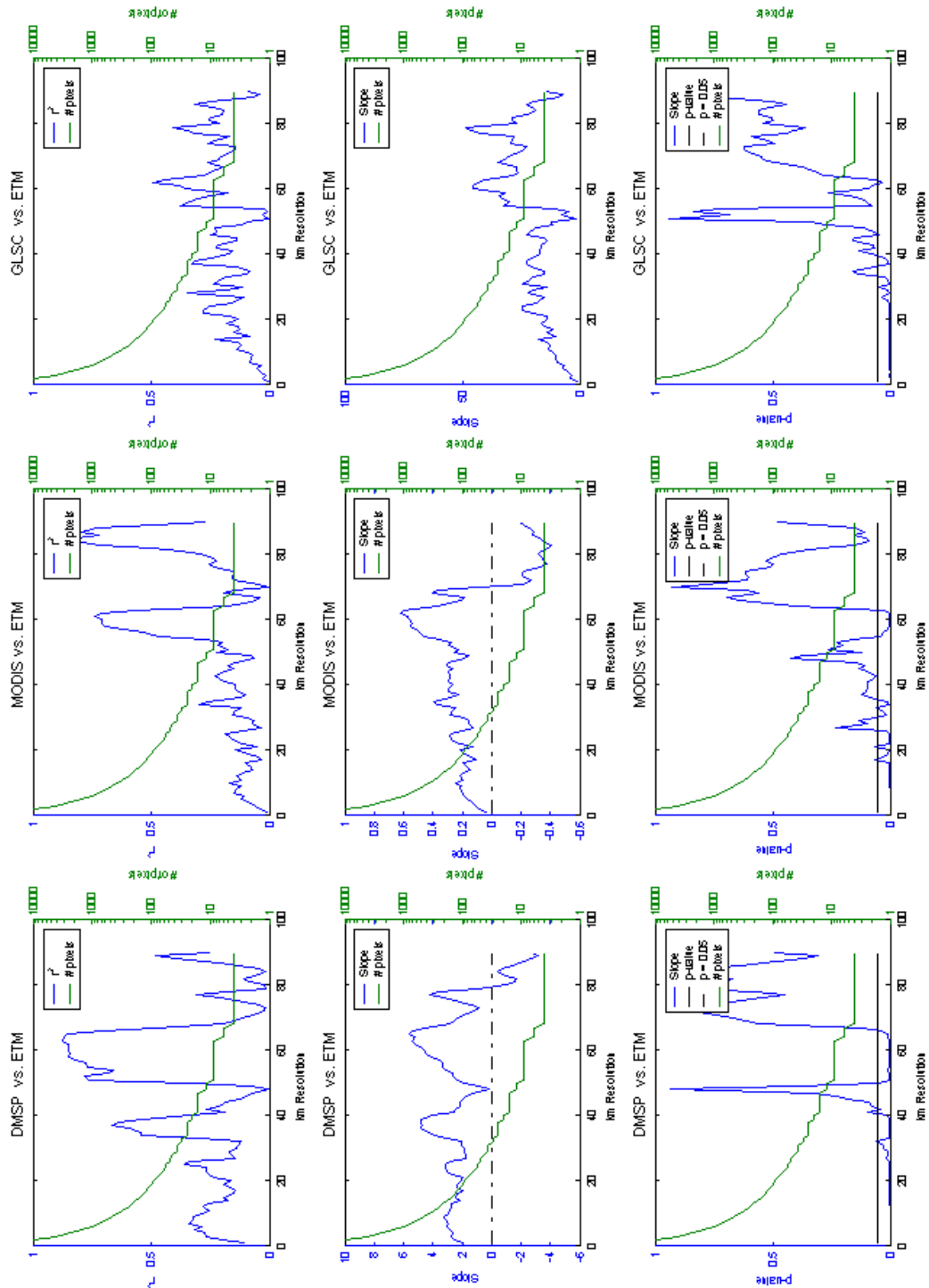


Figure 11: An example of the Modifiable Unit Area Problem (MAUP) and aggregation effect. Plots of linear regression r -squared, regression slope, and p -value as a function of image resolution. The number of pixels used in the regression at a given resolution is plotted on a log scale on each plot, and it can be seen that sudden changes in r^2 , slope, and p tend to occur when a shift in resolution occurs (e.g. between a 3×3 image where $n = 9$ pixels and a 2×2 image where $n = 4$ pixels). Left column: DMSP used to predict burn area. Center column: MODIS used to predict burn area. Right column: GLOBSCAR used to predict burn area.